Mode-selective wavelength conversion based on four-wave mixing in a multimode silicon waveguide

Ding, Yunhong; Xu, Jing; Ou, Haiyan; Peucheret, Christophe

Published in:
Optics Express

Link to article, DOI:
10.1364/OE.22.000127

Publication date:
2014

Document Version
Publisher's PDF, also known as Version of record

Citation (APA):
Ding, Y., Xu, J., Ou, H., & Peucheret, C. (2014). Mode-selective wavelength conversion based on four-wave mixing in a multimode silicon waveguide. *Optics Express*, *22*(1), 127-135. https://doi.org/10.1364/OE.22.000127

Mode-selective wavelength conversion based on four-wave mixing in a multimode silicon waveguide

Yunhong Ding,[*] **Jing Xu, Haiyan Ou, and Christophe Peucheret**

Department of Photonics Engineering, Technical University of Denmark, 2800 Kgs. Lyngby, Denmark
[*]*yudin@fotonik.dtu.dk*

Abstract: We propose and demonstrate all-optical mode-selective wavelength conversion in a silicon waveguide. The mode-selective wavelength conversion relies on strong four-wave mixing when pump and signal light are on the same spatial mode, while weak four-wave mixing is obtained between different modes due to phase mismatch. A two-mode division multiplexing circuit with tapered directional coupler based (de)multiplexers and a multimode waveguide is designed and fabricated for this application. Experimental results show clear eye-diagrams and moderate power penalties for the wavelength conversion of both modes.

OCIS codes: (130.3120) Integrated optics devices; (030.4070) Modes; (130.7405) Wavelength conversion devices; (190.4380) Nonlinear optics, four-wave mixing.

References and links

1. R. Ryf, S. Randel, A. H. Gnauck, C. Bolle, R.-J. Essiambre, P. J. Winzer, D. W. Peckham, A. McCurdy, and R. Lingle, "Space-division multiplexing over 10 km of three-mode fiber using coherent 6×6 MIMO processing," in *Optical Fiber Communication Conference/National Fiber Optic Engineers Conference 2011*, OSA Technical Digest (CD) (Optical Society of America, 2011), paper PDPB10.
2. R. Ryf, S. Randel, N. K. Fontaine, M. Montoliu, E. Burrows, S. Chandrasekhar, A. H. Gnauck, C. Xie, R.-J. Essiambre, P. J. Winzer, R. Delbue, P. Pupalaikis, A. Sureka, Y. Sun, L. Grüner-Nielsen, R. V. Jensen, and R. Lingle, "32-bit/s/Hz spectral efficiency WDM transmission over 177-km few-mode fiber," in *Optical Fiber Communication Conference/National Fiber Optic Engineers Conference 2013*, OSA Technical Digest (online) (Optical Society of America, 2013), paper PDP5A.1.
3. D. J. Richardson, J. M. Fini, and L. E. Nelson, "Space division multiplexing in optical fibers," Nat. Photonics **7**(5), 354–362 (2013).
4. L. H. Gabrielli, D. Liu, S. G. Johnson, and M. Lipson, "On-chip transformation optics for multimode waveguide bends," Nat. Commun. **3**, 1217 (2012).
5. E. Narevicius, R. Narevich, Y. Berlatzky, I. Shtrichman, G. Rosenblum, and I. Vorobeichik, "Adiabatic mode multiplexer for evanescent-coupling-insensitive optical switching," Opt. Lett. **30**(24), 3362–3364 (2005).
6. D. Dai, J. Wang, and Y. Shi, "Silicon mode (de)multiplexer enabling high capacity photonic networks-on-chip with a single-wavelength-carrier light," Opt. Lett. **38**(9), 1422–1424 (2013).
7. Y. Ding, J. Xu, F. Da Ros, B. Huang, H. Ou, and C. Peucheret, "On-chip two-mode division multiplexing using tapered directional coupler-based mode multiplexer and demultiplexer," Opt. Express **21**(8), 10376–10382 (2013).
8. M. Greenberg and M. Orenstein, "Multimode add-drop multiplexing by adiabatic linearly tapered coupling," Opt. Express **13**(23), 9381–9387 (2005).
9. S. Bagheri and W. M. J. Green, "Silicon-on-insulator mode-selective add-drop unit for on-chip mode-division multiplexing," in *Proceedings of IEEE Group IV Photonics Conference* (San Francisco, CA, 2009), paper ThP19.
10. T. Uematsu, Y. Ishizaka, Y. Kawaguchi, K. Saitoh, and M. Koshiba, "Design of a compact two-mode multi/demultiplexer consisting of multimode interference waveguides and a wavelength-insensitive phase shifter for mode-division multiplexing transmission," J. Lightwave Technol. **30**(15), 2421–2426 (2012).
11. J. M. Yates, M. P. Rumsewicz, and J. P. Lacey, "Wavelength converters in dynamically-reconfigurable WDM networks," IEEE Commun. Surv. **2**(2), 2–15 (1999).
12. J. Cheng, M. E. V. Pedersen, K. Charan, K. Wang, C. Xu, L. Grüner-Nielsen, and D. Jakobsen, "Intermodal Čerenkov radiation in a higher-order-mode fiber," Opt. Lett. **37**(21), 4410–4412 (2012).
13. G. Rademacher, S. Warm, and K. Petermann, "Analytical description of cross-modal nonlinear interaction in mode multiplexed multimode fibers," IEEE Photonics Technol. Lett. **24**(21), 1929–1932 (2012).

#199137 - $15.00 USD Received 8 Oct 2013; revised 25 Nov 2013; accepted 28 Nov 2013; published 23 Dec 2013

14. R.-J. Essiambre, M. A. Mestre, R. Ryf, A. H. Gnauck, R. W. Tkach, A. R. Chraplyvy, Y. Sun, X. Jiang, and R. Lingle, "Experimental investigation of inter-modal four-wave mixing in multimode fibers," IEEE Photonics Technol. Lett. **25**(6), 539–542 (2013).
15. Y. Ding, J. Xu, H. Ou, and C. Peucheret, "Mode-selective wavelength conversion based on four-wave mixing in a multimode silicon waveguide," in *39th European Conference on Optical Communication 2013* (London, 2013), paper Tu.1.C.3.
16. A. C. Turner, C. Manolatou, B. S. Schmidt, M. Lipson, M. A. Foster, J. E. Sharping, and A. L. Gaeta, "Tailored anomalous group-velocity dispersion in silicon channel waveguides," Opt. Express **14**(10), 4357–4362 (2006).
17. A. B. Fallahkhair, K. S. Li, and T. E. Murphy, "Vector finite difference modesolver for anisotropic dielectric waveguides," J. Lightwave Technol. **26**(11), 1423–1431 (2008).
18. F. Poletti and P. Horak, "Description of ultrashort pulse propagation in multimode optical fibers," J. Opt. Soc. Am. B **25**(10), 1645–1654 (2008).
19. G. P. Agrawal, *Nonlinear Fiber Optics*, 2nd ed. (Academic, 1995).
20. Y. Ding, L. Liu, C. Peucheret, and H. Ou, "Fabrication tolerant polarization splitter and rotator based on a tapered directional coupler," Opt. Express **20**(18), 20021–20027 (2012).
21. Y. Ding, H. Ou, and C. Peucheret, "Ultrahigh-efficiency apodized grating coupler using fully etched photonic crystals," Opt. Lett. **38**(15), 2732–2734 (2013).

1. Introduction

Mode division multiplexing (MDM) has recently been demonstrated as an efficient mean to increase the communication capacity of single optical fibers in telecommunication systems [1–3]. This technology is also promising in order to increase the capacity of silicon data busses for on-chip optical interconnections [4–10]. MDM may be used to enhance the throughput of the interconnections while limiting the number of required optical sources [4], whose integration onto the silicon platform is still the object of investigations. In future wavelength division multiplexing (WDM) networks, wavelength conversion has been foreseen as an essential functionality [11]. Similarly, in MDM systems also exploiting the wavelength dimension, being able to perform wavelength conversion of the channels would offer new degrees of freedom for the implementation of both fiber and on-chip networks. In this context, intermodal nonlinear interactions in highly-nonlinear fibers (HNLFs) have been recently investigated [12–14], while mode-selective wavelength conversion, which is an important functionality, has not been reported yet.

We have recently proposed and demonstrated a novel all-optical (spatial) mode-selective wavelength conversion based on four-wave mixing (FWM) in a multimode silicon waveguide [15]. In this article, we provide more details on the design and theoretical analysis of the scheme. A tapered directional coupler (DC) based TE_0&TE_1 mode multiplexer is utilized to couple two input channels to two spatial modes of the multimode silicon waveguide. By matching the spatial mode of the pump with that of the signal, idlers are generated from each channel on different modes, and consequently output to different demultiplexing ports. The scheme relies on dispersion engineering of the waveguide, resulting in a strong phase mismatch when the pump and signal are carried on different modes. System experiments are performed to demonstrate the concept using carrier-suppressed return-to-zero (CSRZ) signals at 40 Gbit/s. The experimental results show clear eye diagrams and 1.3 dB and 2.8 dB power penalty for the conversion of each mode taken individually, as well as 2.4 dB and 4.9 dB excess conversion penalty when both signal modes co-propagate in the waveguide.

This article is organized as follows. The principle of mode-selective wavelength conversion and the impact of the phase-mismatch between the different spatial modes are presented in Section 2, together with numerical simulations of the process. Section 3 describes the fabricated multimode silicon waveguide while Section 4 reports the results of mode-selective wavelength conversion experiments at 40 Gbit/s. Finally, the work is concluded in Section 5.

2. Principle and simulation

The principle of on-chip mode-selective wavelength conversion is schematically shown in Fig. 1. Two signal channels, CH_1 and CH_2, are multiplexed to a single multimode silicon

#199137 - $15.00 USD Received 8 Oct 2013; revised 25 Nov 2013; accepted 28 Nov 2013; published 23 Dec 2013

waveguide on mode 1 and 2, respectively. If the pump light is input from the same port as CH_1, it will be coupled to mode 1 in the multimode silicon waveguide, generating a strong idler from CH_1 on the same mode by FWM. On the other hand, if the pump light is input from the same port as CH_2, it will be coupled to mode 2 in the multimode waveguide, generating a strong idler from CH_2 on that mode. The generated idlers will be output to different demultiplexing ports depending on their mode, where they can be spectrally filtered out and detected.

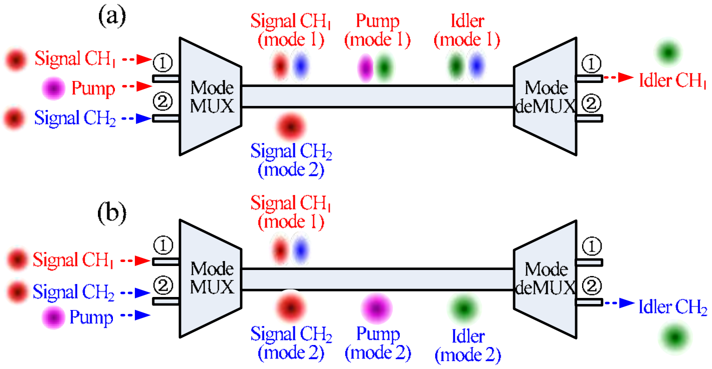

Fig. 1. Principle of mode-selective wavelength conversion based on FWM. Two signal channels CH_1 and CH_2 are multiplexed to a multimode waveguide. Pump light is input from (a) port ① and (b) port ②, generating strong idlers on mode 1 and 2, respectively.

The selective FWM process depends on the phase matching conditions between the interacting waves on the different modes, which are determined by the dispersive properties of the waveguide. Changing the waveguide geometry enables tailoring its dispersion properties [16]. Figure 2 shows the second-order dispersion β_2 for both TE_0 and TE_1 modes of a ridge silicon-on-insulator (SOI) waveguide of height H = 250 nm and different widths calculated by a vectorial finite difference (FD) mode solver [17]. The corresponding phase mismatches for FWM within the TE_0 mode (i.e. where pump, signal and idler are all on the TE_0 mode), FWM within the TE_1 mode, and cross-mode FWM with pump light placed at 1551.7 nm are shown as a function of the signal wavelength in Fig. 3. The phase mismatch parameter is defined as $\Delta\beta = \beta_{\text{signal}} + \beta_{\text{idler}} - 2\beta_{\text{pump}}$, where β_{signal}, β_{idler} and β_{pump} are the propagation constants of the signal, idler and pump, respectively. In order to achieve a high

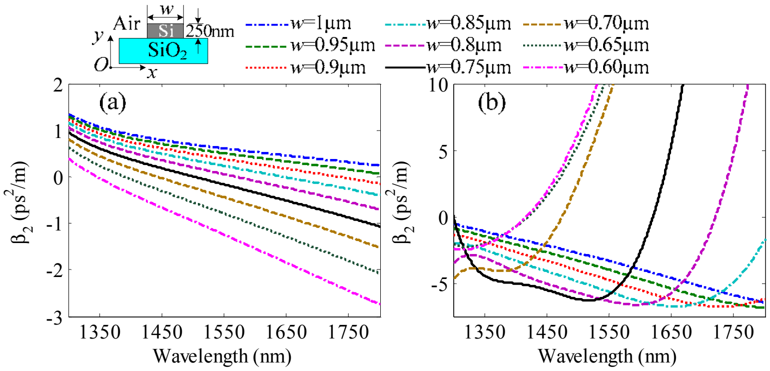

Fig. 2. Second-order dispersion of a silicon waveguide with height of 250 nm and different widths for (a) TE_0 and (b) TE_1 modes.

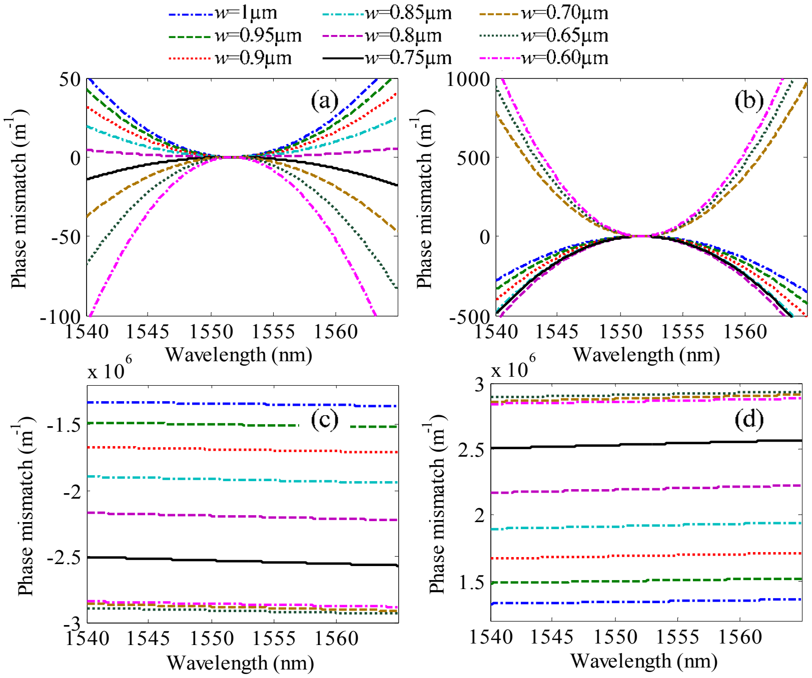

Fig. 3. Calculated phase mismatch as a function of signal wavelength for single-pump FWM with a pump wavelength of 1551.7 nm for (a) TE_0 mode, (b) TE_1 mode, (c) TE_0 mode for the pump, TE_1 mode for the signal, and TE_0 mode for the idler, and (d) TE_1 mode for the pump, TE_0 mode for the signal, and TE_1 mode for the idler.

conversion efficiency for wavelength conversion within both the TE_0 and TE_1 mode, one needs to tailor the dispersion of the multimode silicon waveguide so that the phase mismatch around 1550 nm for those two modes is as small as possible. In addition, the waveguide should maintain a small dimension to increase the optical confinement. In the meantime, in order to keep a low conversion efficiency between the TE_0 and TE_1 modes, a large phase mismatch should be achieved [14]. One can find that, for widths larger than 750 nm, the phase mismatch between the TE_0 and TE_1 modes decreases. On the other hand, for widths smaller than 750 nm, the phase mismatch increases dramatically for both TE_0 and TE_1 modes. As a result, a waveguide width of 750 nm is selected.

FWM in the multimode silicon waveguide is further simulated. Multiple-mode propagation in a nonlinear medium can be described by a multimode nonlinear Schrödinger equation (MM-NLSE) as follows [18]

$$\begin{aligned}\frac{\partial A_p(z,t)}{\partial z} &= i\left(\beta_0^{(p)}-\beta_0^*\right)A_p(z,t)-\left(\beta_1^{(p)}-\beta_1^*\right)\frac{\partial A_p(z,t)}{\partial t}+i\sum_{n\geq 2}\frac{\beta_n^{(p)}}{n!}\left(i\frac{\partial}{\partial t}\right)^n A_p(z,t)+\\ &\quad i\frac{n_2\omega_0}{c}\sum_{l,m,n}\begin{Bmatrix}Q_{plmn}^{(1)}(\omega_0)2A_l(z,t)A_m(z,t)A_n^*(z,t)+\\ Q_{plmn}^{(2)}(\omega_0)2A_l^*(z,t)A_m(z,t)A_n(z,t)\end{Bmatrix} \\ &= D^{(p)}(z,t)+N^{(p)}(z,t)\end{aligned} \tag{1}$$

where A_p is the electric field envelope of mode p. $\beta_n^{(p)}$ is the nth -order dispersion parameter of mode p at frequency ω_0. β_0* and $1/\beta_1$* are free parameters, which are chosen to be the propagation constant and first order dispersion of the pump light in the TE_0 mode. Accordingly, $\beta_0^{(p)}-\beta_0^*$ and $\beta_1^{(p)}-\beta_1^*$ are relative propagation constant and first order dispersion, respectively. $D^{(p)}(z, t)$ and $N^{(p)}(z, t)$ refer to the dispersive and nonlinear operators of the MM-NLSE for mode p, respectively. The nonlinearity $N^{(p)}(z, t)$ couples the mode p to every combination of modes l, m, n. p, l, m, n = 1 or 2 with 1 for the TE$_0$ mode and 2 for the TE$_1$ mode, respectively. c is the velocity of light in vacuum. $Q^{(1)}{}_{plmn}$ and $Q^{(2)}{}_{plmn}$ are overlap integrals dependent on the vectorial mode profile of the waveguide. The effective area for mode combination ($plmn$) is defined as $A_{eff,\ plmn} = 1/(2Q^{(1)}{}_{plmn} + Q^{(2)}{}_{pnml})$. Accordingly, the effective areas of the TE$_0$ and TE$_1$ mode are calculated to be 0.111 μm^2 ($A_{eff,\ 1111}$) and 0.076 μm^2 ($A_{eff,\ 2222}$), respectively. The effective areas for cross-mode coupling are calculated to be 0.131 μm^2 ($A_{eff,\ 1122}$), 0.216 μm^2 ($A_{eff,\ 1212}$), 115.86 μm^2 ($A_{eff,\ 1112}$), and 16.94 μm^2 ($A_{eff,\ 1222}$). In the simulations, the Raman response and self-steepening effect are neglected. The effect of two photon absorption (TPA) is also neglected in the simulations. Considering that the TE$_1$ mode has a stronger energy distribution on the sidewalls of the ridge, the propagation losses for the TE$_0$ and TE$_1$ modes are selected to be 4 dB/cm and 8 dB/cm, respectively. In addition, the nonlinear refractive index n_2 is selected to be 6.3×10^{-18} m^2/W.

The MM-NLSE Eq. (1) is numerically solved by the split step Fourier method [19]. In order to achieve a higher peak power for a given average power and improve the conversion efficiency, the pump light at 1551.7 nm is modulated at 40 Gbit/s in the CSRZ format while the signal light is a continuous wave (CW) at 1554.47 nm. Accordingly, the dispersion parameters are chosen as $\beta_0{}^{(\mathrm{TE0})}–\beta_0{}^* = 0$ ps/m, $\beta_1{}^{(\mathrm{TE0})}–\beta_1{}^* = 0$ ps/m, $\beta_2{}^{(\mathrm{TE0})} = –0.162$ ps^2/m, $\beta_3{}^{(\mathrm{TE0})} = 4.38 \times 10^{-3}$ ps^3/m, and $\beta_0{}^{(\mathrm{TE1})}–\beta_0{}^* = 8.6 \times 10^6$ ps/m, $\beta_1{}^{(\mathrm{TE1})}–\beta_1{}^* = 1.65 \times 10^4$ ps/m, $\beta_2{}^{(\mathrm{TE1})} = –5.87$ ps^2/m, $\beta_3{}^{(\mathrm{TE1})} = –3.67 \times 10^{-2}$ ps^3/m for the TE$_0$ and TE$_1$ mode, respectively. The average powers of pump and signal light are selected to be 20 dBm and 10 dBm, respectively. Figures 4(a) and 4(b) show the simulated intra-mode FWM for the TE$_0$ and TE$_1$ mode, respectively. The corresponding cross-mode FWMs with pump light on the TE$_0$ or TE$_1$ mode, are also shown in Figs. 4(c) and 4(d), respectively. One can find that a strong idler is obtained for both TE$_0$ and TE$_1$ mode FWMs, while the cross mode FWM idler is nearly negligible for pump light on the TE$_0$ and TE$_1$ mode, respectively. The strong harmonic tones visible on the signal spectrum in Figs. 4(a) and 4(b) are due to cross-phase modulation induced by the pump

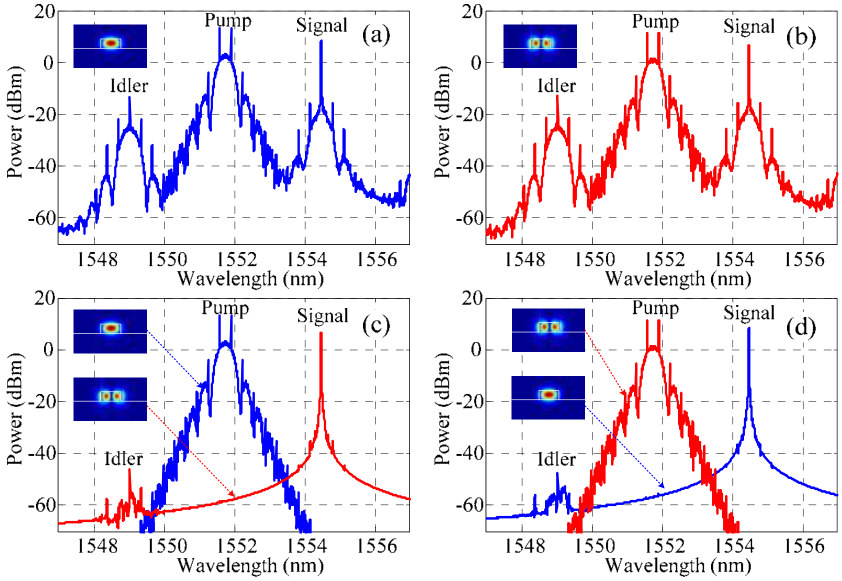

Fig. 4. Simulated spectra of intra-mode FWM for (a) TE$_0$ mode, and (b) TE$_1$ mode, as well as inter-mode FWM with (c) TE$_0$ pump light and TE$_1$ signal light, and (d) TE$_1$ pump light and TE$_0$ signal light. The insets show the distribution of the electric field component $|E_x|$ of the TE$_0$ and TE$_1$ modes for a 750 nm wide silicon waveguide.

light. Therefore our proposed concept of mode-selective wavelength conversion has been validated by numerical simulations.

3. Device fabrication and characterization

In order to experimentally validate our proposal, an on-chip two-mode division multiplexing circuit with 4 mm long straight multimode silicon waveguide [7], as schematically shown in Fig. 5(a), was fabricated on a SOI wafer (top silicon layer: 250 nm, buried silicon dioxide layer: 1 µm). Tapered DCs are used as TE$_0$&TE$_1$ mode (de)multiplexers thanks to their simple structure and larger fabrication tolerance than normal DCs [7, 20]. Fully etched apodized grating couplers [21] are used as input and output ports. A single step of E-beam lithography and inductively coupled plasma reactive ion etching (ICP-RIE) was used for the fabrication. Signals fed to input ports ① and ②, which consist of single-mode TE$_0$ waveguides, are coupled to the TE$_1$ and TE$_0$ modes in the multimode waveguide, respectively, and output from different demultiplexing ports on the TE$_0$ mode. In the tapered DC, the 350 nm wide narrow waveguide is coupled to the wide waveguide, which is tapered from 750 nm to 850 nm with tapering length of 30 µm and coupling gap of 100 nm, as shown in Fig. 5(b). The width of the output of the mode multiplexer (850 nm) is then tapered to 750 nm to match the width of the nonlinear multimode silicon waveguide, as illustrated in Fig. 5(c). In order to accommodate a high input light power, fully etched apodized grating couplers, which are based on photonic crystal structures, as shown in Fig. 5(d), were utilized to couple light to and from the chip. The total insertion losses are 11 dB and 14 dB between input/output ①/① and ②/②, respectively, with mode crosstalk around −15 dB and −12 dB at 1550 nm, as shown in Fig. 6. Note that the insertion losses include the coupling losses to standard single mode fibers (SSMFs) of the grating couplers, as well as the insertion losses of the multiplexer and demultiplexer and the propagation losses of the multimode waveguide. About 3 dB higher insertion loss is measured for CH$_1$ because of the larger multiplexing loss and propagation loss of the TE$_1$ mode compared to that of the TE$_0$ mode.

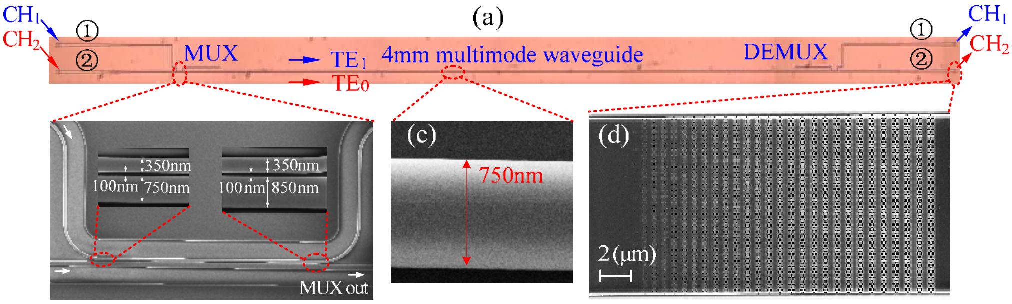

Fig. 5. (a) Microscope image of the two-mode division multiplexing circuit. Scanning electron microscope (SEM) images of (b) a tapered DC based (de)multiplexer, (c) nonlinear multimode silicon waveguide, and (d) an apodized grating coupler. The insets of (b) show the details of the beginning and end sides of the multiplexer.

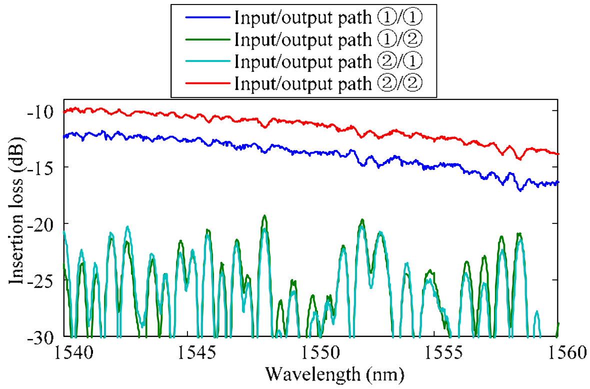

Fig. 6. Measured transmission and mode crosstalk of the two channels (CH_1 and CH_2) of the two-mode division multiplexing circuit.

4. System experiment

The fabricated chip was used to demonstrate mode-selective wavelength conversion with CSRZ signals at 40 Gbit/s. Figure 7 shows the experimental setup. Pump light at wavelength λ_1 = 1551.74 nm is modulated at 40 Gbit/s in the CSRZ format in two cascaded Mach-Zehnder modulators with a pseudo-random binary pattern length of $2^{31}-1$, and then amplified afterward by an erbium-doped fiber amplifier (EDFA). In our demonstration, modulation is imposed onto the pump in order to achieve a higher FWM conversion efficiency. The pump light is then split into two tributaries, each being amplified again by an EDFA and filtered out by an optical bandpass filter (OBPF) for out-of-band noise suppression. A length of 1 km SSMF is used to de-correlate the two pump tributaries. Polarization controllers (PCs) are introduced for each pump tributary to adjust its state of polarization to the TE_0 mode of each input waveguide. Signal light at wavelength λ_2 = 1554.47 nm is also amplified by an EDFA and split into two tributaries with a PC introduced for each tributary in order to excite the TE_0 mode of the input waveguides. Each tributary of pump and signal light are combined by a 3 dB coupler and injected into the silicon chip for FWM. The pump and signal powers input to the chip are about 25 dBm and 12 dBm, resulting in estimated pump and signal powers of about 22 dBm and 9 dBm, respectively, at the input of the nonlinear silicon multimode waveguide. The generated idlers on the TE_0 and TE_1 modes are demultiplexed to different output ports and filtered out by an OBPF, and finally detected in a pre-amplified receiver.

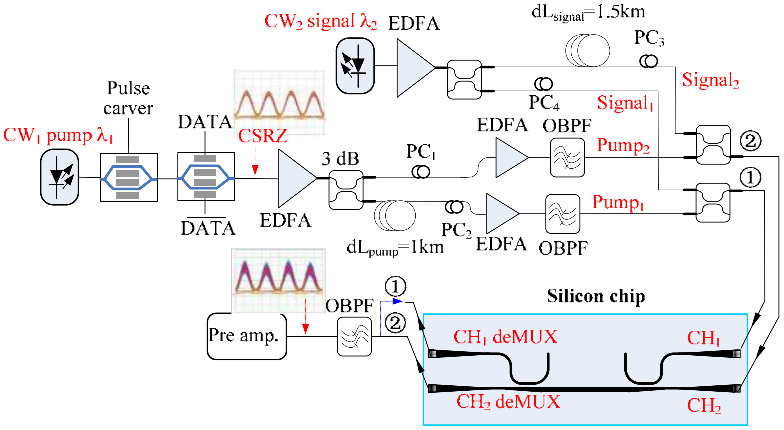

Fig. 7. System experimental setup. The insets show the measured eye-diagrams of the CSRZ signals after the transmitter and that of the filtered idler at one of the outputs of the demultiplexer, respectively.

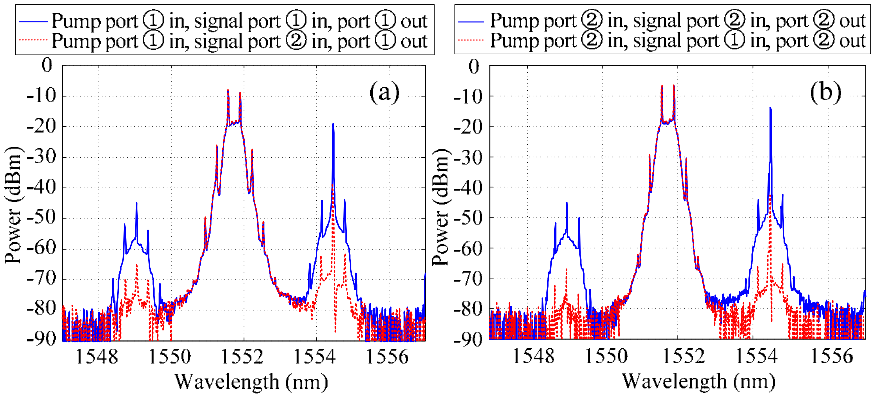

Fig. 8. Spectra measured at (a) ouput port ① for pump input from ①, and signal light input from ① or ②, respectively, and (b) output port ② for pump input from ①, and signal light input from ① or ②, respectively.

Figures 8(a) and 8(b) show the measured FWM spectra at output ports ① and ②, respectively, when the pump light is input from input ports ① and ②, respectively, and the signal is input at either port ① or port ②. Crosstalk induced by residual FWM (pump light is input from input port ① and ②, signal light is input from input port ② and ①, and detected at output port ① and ②, respectively), which is caused by leakage light in the TE$_0$&TE$_1$ mode multiplexer, is also represented. Strong FWM is obtained when signal and pump lights are injected into the same multiplexing port. Meanwhile, very weak residual FWM is obtained if pump and signals are input from different multiplexing ports. The modal crosstalk on the idlers is better than 20 dB for both modes. The modal crosstalk is contributed by the multiplexer, where signal light input to the port that is different from the one where the pump is injected leaks to the same mode as the pump light in the multimode waveguide.

Figure 9 shows the results of bit-error-ratio (BER) measurements performed for the two idlers obtained at output port ① (corresponding to idler on the TE$_1$ mode) or output port ② (corresponding to idler on the TE$_0$ mode) when pump and signal light are simultaneously input from input port ① or input port ②, respectively (i.e. in the absence of modal crosstalk),

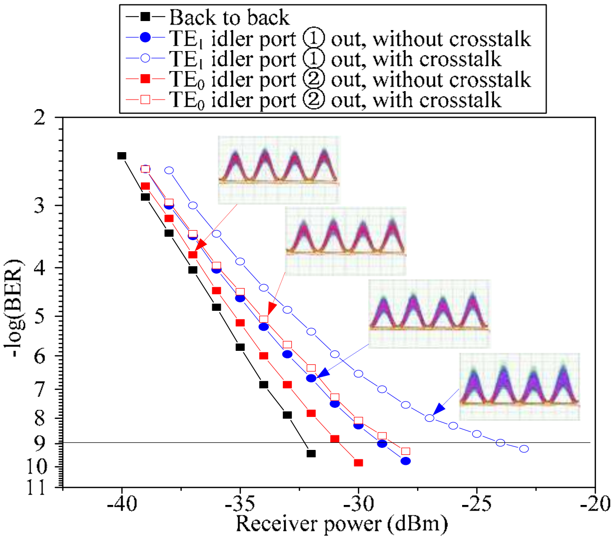

Fig. 9. BER measurement for the TE$_0$ and TE$_1$ idlers output from demultiplexing port ① and ②, respectively, with and without crosstalk, and the corresponding eye-diagrams.

as well as when signals are simultaneously input to ports ① and ② (i.e. in the presence of crosstalk). The corresponding eye-diagrams are also shown in the figure. Clear eye-diagrams are obtained for the idlers with and without crosstalk. In the absence of crosstalk, power penalties of 1.3 dB and 2.8 dB compared to the back-to-back case are obtained for the idlers output from port ① and ②, respectively. An extra 2.4 dB and 4.9 dB power penalties are obtained with crosstalk, respectively.

5. Conclusions

We have successfully demonstrated on-chip mode-selective wavelength conversion based on FWM in a multimode silicon waveguide using a two-mode division multiplexing circuit. Mode-selectivity is realized by launching pump light on different spatial modes, resulting in good phase matching, hence high conversion efficiency, when the modes of the pump and signal coincide. In contrast a large phase mismatch is obtained when the pump and signal are supported by different spatial modes, resulting in poor conversion efficiency. Experimental results show clear eye diagrams for conversion of the two modes with and without crosstalk and power penalties of 1.3 dB and 2.8 dB for the conversion of each mode taken individually, as well as 2.4 dB and 4.9 dB excess conversion penalty with crosstalk. The method could possibly be extended to a larger number of modes, provided the multimode silicon waveguide remains sufficiently nonlinear and optimum phase matching conditions can be found in order to scale intra- and inter-modal FWM.